Simulation of the two-stream convective instability

J. Busnardo-Neto and J. E. Rowe

Electron Physics Laboratory, Department of Electrical and Computer Engineering, The University of Michigan, Ann Arbor, Michigan 48104

(Received 18 January 1973; final manuscript received 9 October 1973)

A ring/disk model is used in numerical experiments to investigate the two-stream convective instability in a cylindrically symmetric system with finite transverse dimensions. The spatial growth rates obtained in the linear region agree well with the predictions of the linear theory. The development of a vortex structure in velocity-phase space is associated with the saturation of the instability. Generation and amplification of harmonics occur abundantly as expected. The two electron streams exchange kinetic energy over a very short distance and become thoroughly mixed and randomized (thermalized). Due to the choice of geometry, no coherent oscillations are established in the transverse plane, and although they increase, the radial and angular kinetic energies remain much less than the axial.

I. INTRODUCTION

The use of computer models to study phenomena that occur in plasmas has become well established during the past decade.[1-4] These models are well suited for numerical experiments in which time is the independent variable, and they have been extensively used to investigate absolute instabilities, usually in infinite systems with periodic boundary conditions, although some studies of finite-length systems are also reported in the literature.[5] The development in space of a convective instability can be studied using models similar to the ones mentioned here, but now distance is the independent variable and periodicity in time is assumed. These models were originally developed by traveling-wave tube workers who were interested in gain saturation and harmonic distortion that are due to the nonlinear behavior of the electron beam in high-power efficient devices.[6] The steady state of beam-plasma instabilities was studied with this nonlinear model for the beam while the plasma was treated linearly, either as a dielectric[7] or as a slow-wave structure.[8] Obviously, nonlinear effects could be observed only in the beam. Mihran and Yu[9] investigated noise generation in multivelocity electron beams with this model. Mihran[10] then reduced the velocity classes to two and studied the two-stream instability obtaining good agreement between initial growth rates predicted by the linear theory and those observed in the computer experiments.

A convective instability appears when two streams of charged carriers travel in the same direction, with the difference of their drift velocities greater than the sum of their thermal velocities. We investigated this instability by means of numerical experiments, using the Lagrangian formulation developed by Rowe,[11] in which the charges are represented by disks or rings of specified dimensions and charge density. Cylindrical symmetry is assumed and the streams are surrounded by a perfectly conducting drift tube. The geometry is shown in Fig. 1. The streams are concentric, have the same diameters, and are cold initially. A uniform magnetic field in the axial direction permeates the interaction region and only slow waves are considered. The system is open-ended and a perfectly matching termination can be placed anywhere along the drift tube. The streams are made up of electrons and a fixed neutralizing background may or may not be present. A steady state in time is assumed with all dependent variables having a period $2\pi/\omega$. The instability is excited by a velocity or density modulation of frequency $\omega/2\pi$ applied at the initial plane. The growth of the harmonic spectrum of these excitations with distance, the saturation of this growth and the exchange of energy between the streams are the aspects of the instability that have been investigated. A total of nine numerical experiments were completed. We report the results of two experiments with a complete two-dimensional model and the results of three experiments with a simplified one-dimensional version of the model in which all motion is restricted to the axial direction.

II. THE MATHEMATICAL MODEL

In the Lagrangian formulation both streams are divided into a number of charged particles whose trajectories are followed throughout the interaction region. In the present axially-symmetric, two-dimensional treatment these particles are rings with the same charge and charge-

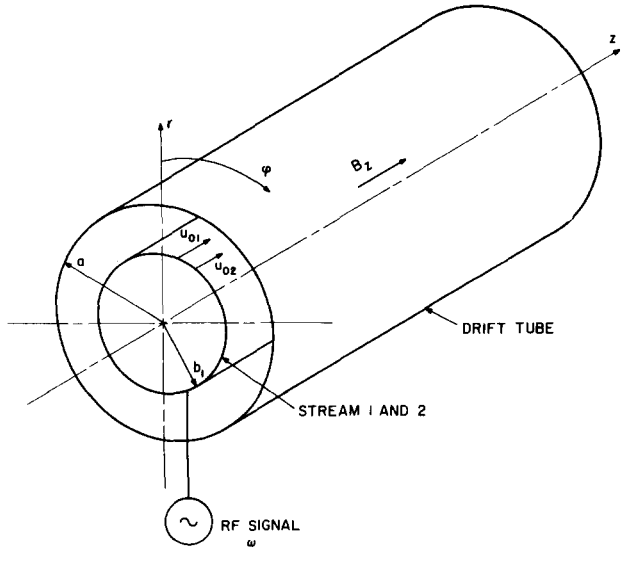

FIG. 1. Two-stream interaction configuration with $b = 0.8\,u_0/\omega$ and $a = 1.6\,u_0/\omega$. The first stream has drift velocity $u_{01}(1 + b)$, the slow one has drift velocity $u_{02}(1 - b)$.

to-mass ratio as the electron. The particles are also referred to as rings or even simply electrons. The rings are identified by the stream they belong to, by their entrance radius r_0 and by their time of arrival t_0 at the entrance plane $z = 0$. Thus, the independent variables in this formulation are r_0, t_0, and the axial coordinate z. The dependent variables are the axial, radial, and angular velocities, the radial position and the time of arrival of the particles at the position z. These variables are called the microscopic dependent variables since they provide information at the particle level.

With the assumptions mentioned previously, each particle is acted upon by the Lorentz force only, and in cylindrical coordinates Newton's second law is written, in component form, as

$$\frac{d^2z}{dt^2} = -\eta E_z, \tag{1}$$

$$\frac{d^2r}{dt^2} - r\left(\frac{d\phi}{dt}\right)^2 = -\eta\left(E_r + rB_z\frac{d\phi}{dt}\right), \tag{2}$$

and

$$\frac{1}{r}\frac{d}{dt}\left(r^2\frac{d\phi}{dt}\right) = \eta B_z\frac{dr}{dt}, \tag{3}$$

where η is the charge-to-mass ratio of the electron (a positive number), B_z is the uniform magnetic flux density applied in the axial direction, and E_z and E_r are the axial and radial components of the electric field due to the charges of all other particles. To make all quantities convenient for computer calculation, we introduce the following normalizations for the independent variables:

$$y\Delta\frac{S\omega}{u_0}z, \quad x_0\Delta\frac{S\omega}{u_0}r, \quad \Phi_0\Delta - \omega t_0,$$

where u_0 is the average of the drift velocities of the streams, ω is the radian frequency corresponding to the basic time period, S is an arbitrary scale factor, y is the normalized distance, and x_0 and Φ_0 are the normalized initial radial and phase positions of a particle. The velocities and the radial position of the particles are normalized as follows:

$$v_z = \frac{dz}{dt}\Delta u_0(1 \pm b)[1 + 2Su_y(y, x_0, \Phi_0)],$$

$$v_r = \frac{dr}{dt}\Delta u_0[2Su_x(y, x_0, \Phi_0)],$$

$$v_\phi = \frac{d\phi}{dt}\Delta u_0\left(\frac{2S}{r}u_\phi(y, x_0, \Phi_0)\right),$$

$$x(y, x_0, \Phi_0)\Delta\frac{S\omega}{u_0}r.$$

Here, $1 + 2Su_y$ is the normalized axial velocity, $2Su_x$ is the normalized radial velocity, $2Su_\phi$ is the normalized angular velocity, and x is the normalized radial position. These are the velocities and the radial position that each particle has at the time it arrives at a fixed plane $y = \text{const}$. In the expression $(1 \pm b)$, the upper sign refers to stream 1 and the lower one to stream 2. Stream 1 is the fast one, with average velocity $u_{01}\Delta u_0(1 + b)$; stream 2 is the slow one, with average velocity $u_{02}\Delta u_0(1 - b)$. The velocity separation parameter b is small compared with one. The remaining dependent variable is the arrival time of each particle at a plane y, and we introduce a phase variable to express this time as

$$\Phi(y, x_0, \Phi_0)\Delta\frac{\omega}{u_0}z - \omega t = y/S - \omega t. \tag{4}$$

At each fixed plane $y = \text{const}$, Φ represents the time distribution of the particles, and it is a dependent variable which has a period 2π. Equation (4) can be rearranged to read $(u_0/\omega)\Phi = z - u_0 t$, and it is then seen that Φ can also be thought of as a measure of the position of a particle in a frame of reference moving with the average drift velocity u_0.

In terms of the normalized variables, the equations of motion become

$$\frac{\partial u_y}{\partial u}(1 + 2Su_y) = \frac{1}{(1 \pm b)^2}E_y(y, x, \Phi), \tag{5}$$

$$\frac{\partial u_x}{\partial y}(1 + 2Su_y) = \frac{1}{1 \pm b}E_x(y, x, \Phi) + \frac{1}{(1 \pm b)}\frac{2S}{x}u_\phi^2 - \frac{1}{1 \pm b}\left(\frac{\omega_c}{S\omega}\right)u_\phi, \tag{6}$$

and

$$\frac{\partial u_\phi}{\partial y}(1 + 2Su_y) = \frac{1}{1 \pm b}\left(\frac{\omega_c}{S\omega}\right)u_x - \frac{1}{1 \pm b}\frac{2S}{x}u_\phi u_x, \tag{7}$$

where $\omega_c\Delta\eta B_z$ is the cyclotron frequency and E_y and E_x are the normalized fields which are defined in the appendix. In obtaining (5), (6), and (7) the following operator was used:

$$\frac{d}{dt} = \frac{dz}{dt}\frac{\partial}{\partial z} = u_0(1 \pm b)\frac{S\omega}{u_0}(1 + 2Su_y)\frac{\partial}{\partial y},$$

which is the convective derivative following the motion of a particle. This operator is also applied to (4), which defines Φ, to obtain the equation for the phase positions:

$$\frac{\partial\Phi}{\partial y} = \frac{1}{S}\left(1 - \frac{1}{(1 \pm b)(1 + 2Su_y)}\right). \tag{8}$$

The radial position of a particle at the displacement plane y is obtained from

$$x = x_0 + \int_0^y \frac{2Su_x(y', x_0, \Phi_0)}{(1 \pm b)[1 + 2Su_y(y', x_0, \Phi_0)]}dy', \tag{9}$$

which is the integral of the incremental radial displacements along the trajectory of the particle. The prime denotes the integration variable. Equations (5)–(9) determine the velocities, the radial position, and the time of arrival of each particle at a plane y. The distance between any two particles can be calculated from their known velocities and time of arrival.[6,9] The field acting on any one particle is computed by adding up the contributions of all other particles and these contributions depend only on the distance between the particles. The field is then used in the force equations to advance the particle one distance step. The process is repeated for all particles so that there are at least as many field computations per distance step as there are particles. Note that the field can be computed at any (x, Φ) position, and indeed, this is

done over a uniform (x, Φ) grid for output and diagnostic purposes.

The accuracy of the model is determined by the integration step and the number of particles used. Several test runs were made using either one half or twice the standard number of particles and also doubling and halving the distance step. No significant differences in the results were observed as a result of these tests. Another test of the accuracy of simulation models, and one that is widely used, is the conservation of the total energy. Also, in a cylindrically symmetric system, the canonical angular momentum is a constant of the motion. Both of these two conservation theorems represent known integrals of the differential equations that are being integrated numerically. They, therefore, provide a check on the numerical accuracy of the model that is used and if not satisfied, then the number of particles in the simulation would have to be increased, or the integration step would have to be reduced, or maybe both. In our experiments, the total energy was conserved within 0.5% and the canonical angular momentum was conserved within a few percent.

The formulation of the two-stream instability presented here can be considered as a microscopic approach to the problem. The integration of the differential equations yields the radial position, the three velocities, and the phase position of every particle at each plane y. This constitutes a great amount of detailed information and appropriate averages and integrations are required. These are called the macroscopic dependent variables and the ones that we considered are the electric fields, the harmonic currents, the kinetic energy, the average velocities, and the thermal velocities (standard deviation of the velocities). The behavior of the macroscopic variables with distance and in some cases the behavior of the microscopic variables with time at a fixed plane constitute the bulk of our results and are presented as computer-generated plots in the next section.

III. RESULTS OF NUMERICAL EXPERIMENTS. ONE-DIMENSIONAL MODEL

A simplified, one-dimensional version of the model described in the previous section can be obtained if all motion is restricted to the axial direction. This corresponds to the experimental situation in which a very large applied magnetic field effectively inhibits all transverse motion. The particles now are disks of charge of radius b_1 and of finite thickness. The pertinent equations for this case are the axial force equation (5) and the equation for the phase of the particles (8). Appropriate modifications are introduced in the computation of the normalized axial field E_y and they are described in the appendix In the three numerical experiments reported here, the two streams have the same charge density, which is specified by their plasma frequencies as $\omega_{p1}/\omega = \omega_{p2}/\omega = 0.1$; the velocity separation parameter was chosen as $b = 0.05$; the radius of the streams is given by $b_1 = 0.8u_0/\omega$ and the radius of the drift tube by $a = 1.6u_0/\omega$. In the one-dimensional case, the transverse dimensions should be small compared with the electronic wavelength $2\pi u_0/\omega$. The scale factor S is chosen so that the distance is normalized to $\lambda_q/2\pi\Delta u_0/\omega_q$, where $\omega_q = R\omega_p$ is the re-

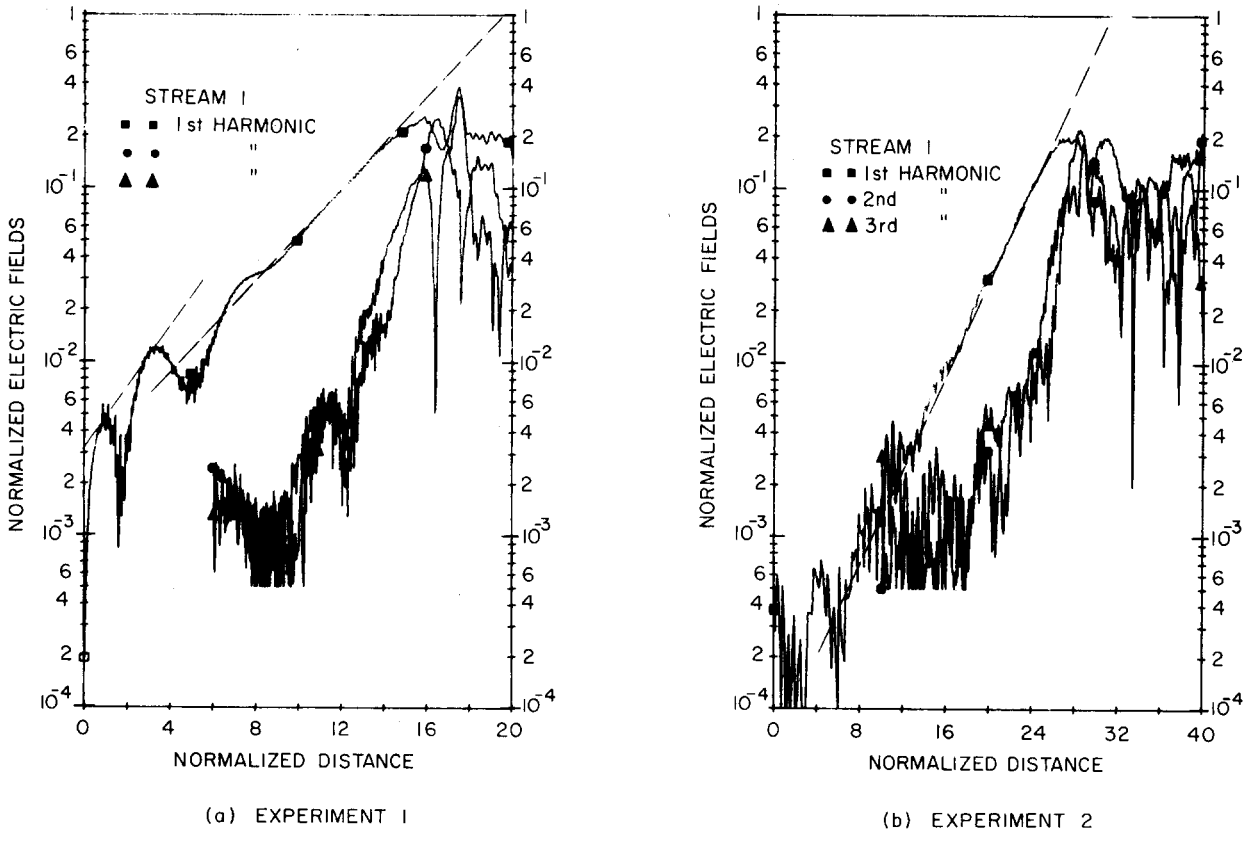

FIG. 2. Electric field harmonics vs distance. (a) Experiment 1, 0.1-percent initial velocity modulation; (b) Experiment 2, 0.1-percent initial density modulation.

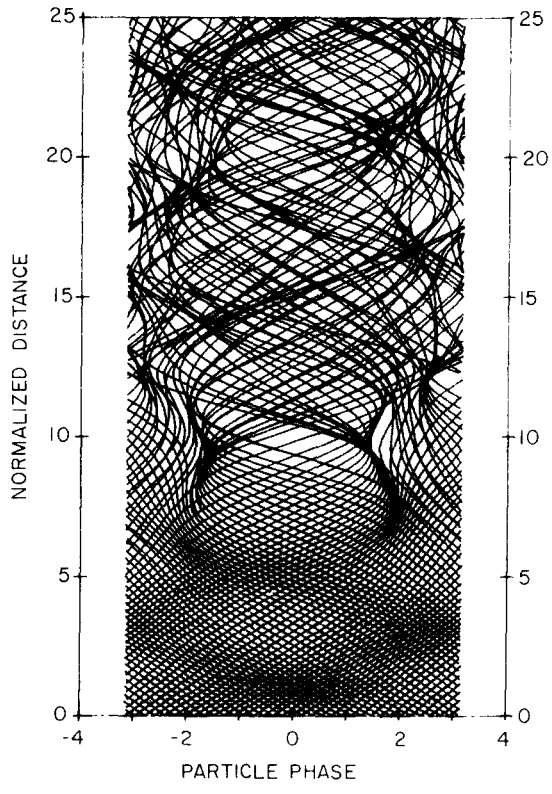

FIG. 3. Flight-line diagram for experiment 3. (One-percent initial velocity modulation.)

duced plasma frequency corresponding to the total charge density. Here, $\omega_p^2 = \omega_{p1}^2 + \omega_{p2}^2$ and R is the plasma-frequency reduction factor.[12] The integration step used was $\Delta y = 0.01$, that is, approximately 600 steps were taken for each reduced plasma wavelength. Each stream was simulated by 35 disks distributed over one period $2\pi/\omega$ of the perturbation that excites the instability.

The difference between the experiments lie in the way the instability is excited. In experiment 1 the initial velocities are given by $u_0(1 \pm b)(1 + 0.002 \sin \Phi_0)^{1/2}$ which corresponds to a 0.1% modulation of each stream through a klystron grid (velocity gap); in experiment 2 there was no velocity modulation, but an initial phase modulation was applied, corresponding to a sinusoidal density modulation of 0.1% at the frequency ω; in experiment 3 the depth of the velocity modulation was increased to 1%. The growth with distance of the harmonic spectrum of the excitations is the main aspect of the interaction to be investigated. With these low modulation levels it was observed that the various modes excited by the imposed modulations disappear rapidly except for the fastest growing one. A region of clear exponential growth of the harmonics of the electric field and the current appeared in experiments 1 and 2. The growth rate measured from Fig. 2 is 0.31, which compares well with the linear prediction of 0.327, which was obtained from a solution of the cold plasma, one-dimensional dispersion relation, which included the reduction factor R.[12,13] For the cases with initial velocity modulation there exists a high initial growth that is due to a klystron-like bunching mechanism. This produces a very rapid increase in the fields and currents in the beginning of the interaction and only after that does the two-stream mechanism become dominant. In experiment 3 when the two-stream instability takes over the fields and currents are already too high and the nonlinearities destroy the region of exponential growth. This rapid initial growth seen in experiments 1 and 3 was not present in experiment 2 since the density modulation leads to debunching, instead of bunching [Fig. 2(b)]. The end result is that it takes longer for saturation to occur with an initial density modulation even though the exponential growth rate is the same and the same level of current modulation is used. Note that the region of exponential growth in experiment 2 begins at a level one order of magnitude lower than in experiment 1. Eventually, the nonlinearities of the system stop the growth of the instability, and it was observed that at this point the first five harmonics of the electric field have the same amplitude (0.2 normalized units) in all three experiments. This occurs despite the fact that the initial velocity modulation excites several harmonics which lie outside of the growth region of the linear theory and that the initial density modulation was carefully prescribed so as to excite only the fundamental. We believe that this amplification and generation of harmonics is due to the nonlinearities in the two-stream instability. The harmonics of the currents behave in exactly the same manner as the harmonics of the fields in all three experiments. Again at saturation all harmonics have the same amplitude, 0.5 normalized units. This last result agrees with those reported by Mihran.[10] The post-saturation region is characterized by an oscillatory behavior of the harmonics of the currents and of the field.

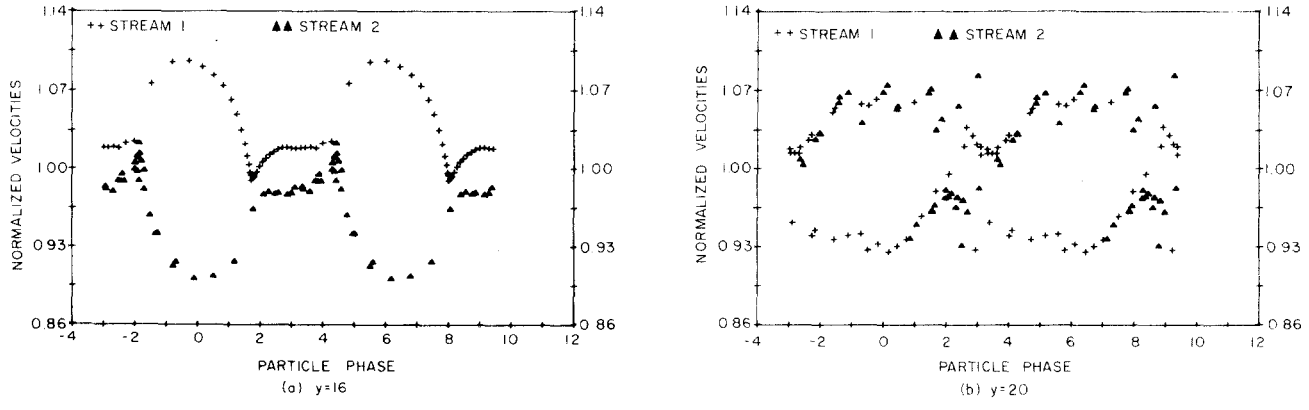

FIG. 4. Normalized velocities vs phase (time) at two fixed planes. (Experiment 1, 0.1-percent initial velocity modulation).

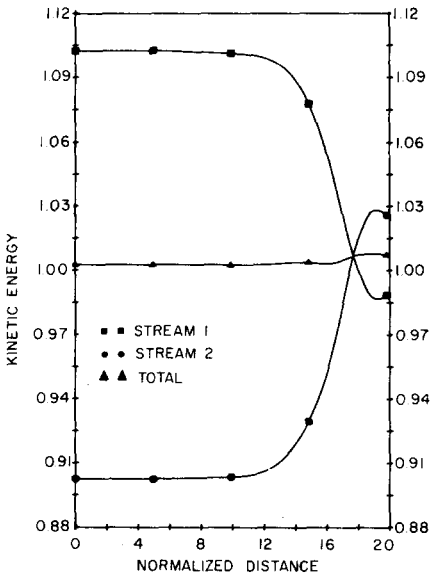

FIG. 5. Average kinetic energy of particles on stream 1, on stream 2 and for the entire system. (Experiment 1, 0.1-percent initial velocity modulation).

No decay in the amplitudes was seen.

Observation of the flight-line diagrams (phase of the particles plotted vs distance) leads us to the conclusion that saturation of growth occurs when trapping occurs, i.e., when particles cannot be added to the potential troughs of the wave and are reflected. The strong trapping center that appeared around $y = 9$ in experiment 3 is shown in Fig. 3. Farther along the interaction region, the ordered behavior of the phases of the particles with distance disappears completely and the particles oscillate with distance. This region of disorder is very similar to those described by Buneman.[1] When trapping occurs some particles in stream 1 are slowed below the average drift velocity u_0 and some particles in stream 2 are speeded up above u_0. This process should also be visible in velocity vs phase plots and Fig. 4 shows two of these plots for experiment 1 (trapping now occurring first at $y = 16$). This vortex structure in velocity-phase space is typical of the two-stream interaction and has been observed by several authors.[3,5,14] In our case, the vortices are stable and were clearly visible in all experiments until the computer runs were interrupted at a point two reduced plasma wavelengths after saturation. This spreading in velocity space is reflected in the form of the velocity distribution function at several fixed planes. At the initial plane, the two streams are cold and the distribution function has two sharp peaks. As the vortex structure develops the peaks broaden and when the vortex is fully formed slow and fast tails appear around $0.9u_0$ and $1.1u_0$. At the end of the interaction, the two streams are thoroughly mixed and have coalesced into a single one with a broad distribution function. The spread of the distribution function is measured by the standard deviation of the velocities. Here we refer to the thermal velocity even though the total number of particles (70) is too small to warrant any statistics. In all three experiments where the vortex was fully formed and saturation occurred, the thermal velocities of both streams were equal to the velocity separation parameter b. This corresponds to the prediction of the linear theory that growth occurs only if the sum of the thermal velocities of the streams is less than the difference of their mean drift velocities.

The thermalization of the streams occurs at the expense of their ordered kinetic energy and in all experiments the fast stream loses energy to the slow stream and in the end all kinetic energies are equal (Fig. 5). The total kinetic energy changes very little even though the energy stored in the electric field grows by several orders of magnitude. This is explained by the fact that the electrostatic energy is much smaller than the kinetic energy. The total energy of the system is conserved within 0.2% in all one-dimensional experiments, and this is taken as an indication of the accuracy of the model. The kinetic energy of each stream remains constant for a long distance even though the electric field and currents are growing by orders of magnitude. However, the exchange of kinetic energy between the streams is very fast, occurring in less that one reduced plasma wavelength once it begins. Also, there is an "overshoot" and the average kinetic energies tend to the total average kinetic energy with small oscillations. The sudden exchange of kinetic energies is associated with an intriguing result of the Fourier analysis of the electric field. This is shown in Fig. 6 where the dc components of the fields acting on stream 1 and on stream 2 are plotted vs distance. These do not have any meaning as an average electric field and are interpreted as the time-averaged acceleration of the disks in stream 1 and stream 2. Throughout the region where growth occurs, the average accelerations are zero but immediately before saturation stream 1 is subjected to a high decelerating force while stream 2 is accelerated. These strong pulses exist for a very short distance (approximately one third of the reduced plasma wavelength) and decay into an oscillatory behavior around zero. The pulses end exactly at the point where the kinetic energies of the two streams first become equal. We believe that

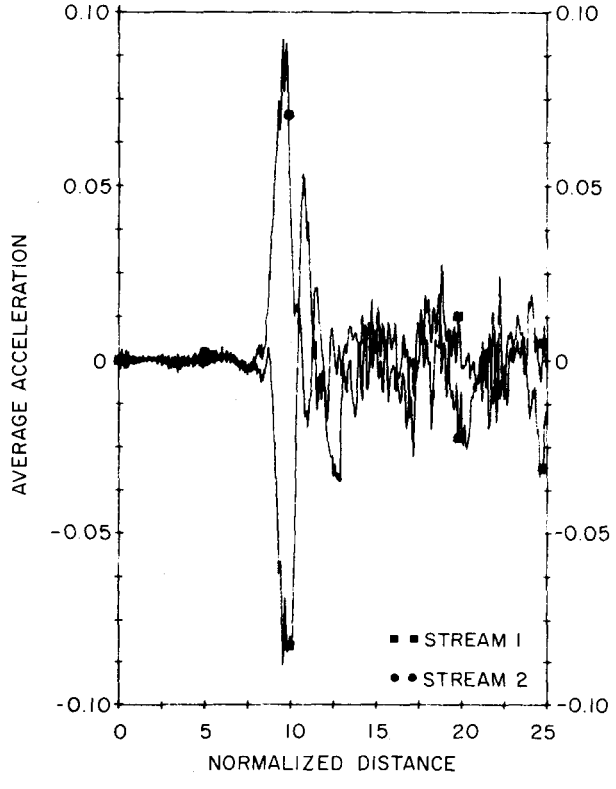

FIG. 6. Average acceleration on particles of stream 1 and stream 2. (Experiment 3, one-percent initial velocity modulation).

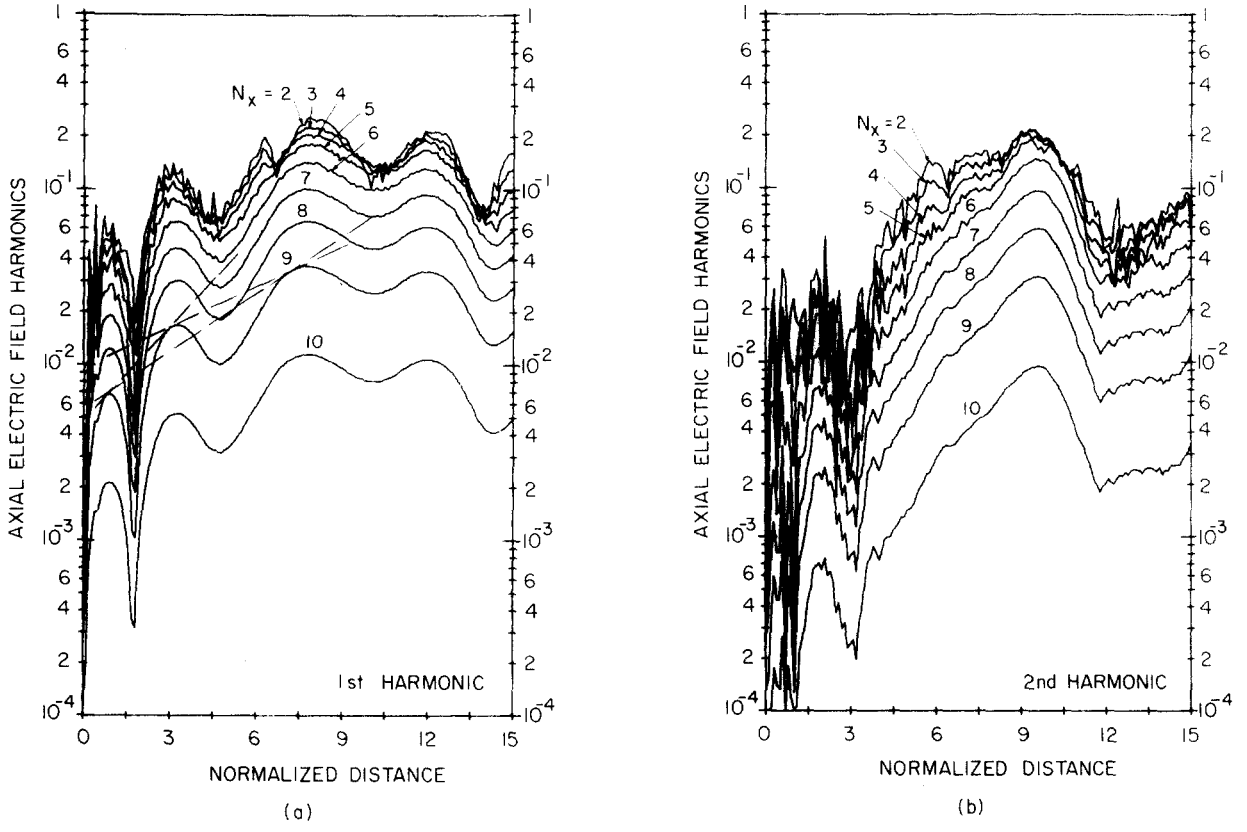

FIG. 7. Harmonics of the axial electric field at each of the radial positions for experiment 4. ($M = 32$, $N = 3$, $N_x = 10$, $N_\Phi = 32$, $\omega_{p_1}/\omega = \omega_{p_2}/\omega = 0.1$, $\omega_{c_1}/\omega = 0.24$).

these strong and sudden effects are due to the formation of the vortex structure in velocity space, since the pulses begin when the first particles are trapped and they go through their maximum value when the particles of both streams are first spread out over the entire range of velocities attained. This is also the point where the vortex goes through a maximum and the slow and fast tails are very clear in the velocity distribution function. At the moment, we are unable to advance a reasonable explanation for these observations.

IV. RESULTS OF NUMERICAL EXPERIMENTS. TWO-DIMENSIONAL MODEL

In the two numerical experiments with the complete two-dimensional model, we used the same parameters and the same type of excitation as in the experiments described in Sec. III. This allows us to check whether any of the previous results are due to the simplifications involved in reducing the problem to a one-dimensional formulation. Again, the distance is normalized to u_0/ω_q and integration steps equal to 0.01 and 0.02 were used, which satisfy the requirement of being much smaller than both the reduced plasma wavelength and the cyclotron wavelength ($\omega_c/\omega = 0.24$) very well. Each stream is divided into N annular layers of charge and each layer in turn is divided into M particles per period for a total of $2N \times M$ rings. Two choices of N and M were used: experiment 4 has $N = 3$ and $M = 32$; experiment 5 has $N = 10$ and $M = 16$. For output purposes, the radial direction is divided equally into N_x space-charge layers and the time period into N_Φ equally spaced points. For diagnostics and output purposes, the electric fields are computed on this (x, Φ) grid usually every 10 integration steps, but when advancing the particles, the fields are computed at the actual radial and phase positions of the rings. Experiment 4 has $N_x = 10$ and $N_\Phi = 32$; experiment 5 has $N_x = 20$ and $N_\Phi = 16$. Either choice of N, M, N_x, and N_Φ is not totally satisfactory but the number of particles (192 and 320) had to be kept reasonable due to the cost of the computer runs. On an IBM 360/67, experiment 4 took 800 sec for 100 steps (one distance unit, $\Delta y = 0.01$) and experiment 5 took 1200 sec for 50 steps (one distance unit, $\Delta y = 0.02$). As one might suspect, experiment 4 gives better results in the axial direction while experiment 5 gives better results in the radial direction.

In general, all the results obtained with the one-dimensional model are confirmed here. These include the growth rates, the particular way in which the fields grow, the point where saturation occurs, and the values of the fields at saturation. The harmonics of the axial and radial fields show some "noise" (Figs. 7 and 8), and we believe that this is due to the relatively small number of particles used. The fields for experiment 5, with half the number of particles per time period are even "noisier." The numbers indicate the radial position where the fields are computed. The streams do not spread much farther out than $x = 0.05$, therefore, curves labeled 2-5 represent fields measured inside the streams and curves labeled 6-10 represent fields measured outside. Both the axial and radial fields are smoother outside the streams and this is also observed in the plots of the fields vs time (phase). It

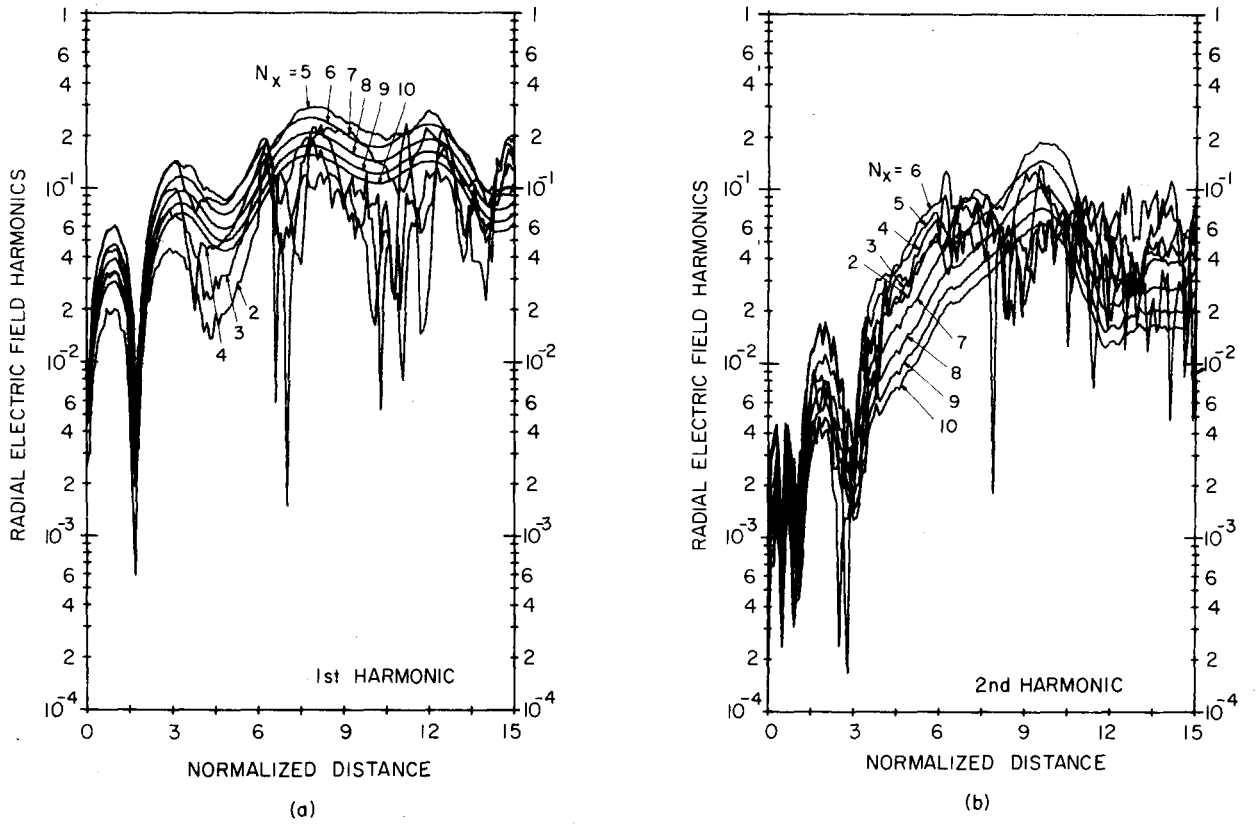

FIG. 8. Harmonics of the radial electric field at each of the radial positions for experiment 4. ($M = 32$, $N = 3$, $N_x = 10$, $N_\Phi = 32$, $\omega_{p_1}/\omega = \omega_{p_2}/\omega = 0.1$, $\omega_c/\omega = 0.24$).

seems that the harmonics saturate earlier inside the streams. The axial fields are strongest inside the streams and vary little with radial position which would justify the use of one-dimensional models. Plots of the axial velocities vs phase show the development of the vortex structure although with a smaller range of velocities. The vortices are very clear and seem to be stable, and we did not notice the qualitative changes when going from one to two dimensions that were observed by Morse and Nielson in their time-dependent experiments.[3] The axial velocity distribution function shows the slow and fast tails and the dip in the middle that are characteristic of the persisting vortex structure. The saturation of growth and vortex structure are associated with the trapping that can be seen in the flight-line diagrams (trajectories of the particles). Trapping occurs earlier close to the axis and farther and farther down the streams for increasing radial distances (Fig. 9, similar plots for experiment 5 are not shown). The change of the trapping distance with radius plus the earlier saturation of growth inside the streams indicate that the instability is stronger closer to the axis. Plots of the axial kinetic energy, computed for each layer of each stream vs distance add evidence to this conclusion (Fig. 10). The inner layers exchange energy in a way similar to the one-dimensional experiments while the outer layers interact weakly and little energy is either gained or lost by them.

However, in the two-dimensional case the total exchange of axial kinetic energy is less pronounced than in the one-dimensional experiments and stream 1 remains the fast stream and stream 2 the slow one. The possibility of radial motion effectively destroys the strong axial effects of the instability. It might be expected then that the axial kinetic energy would be reduced while the radial and angular kinetic energies would show marked gains. The mechanism would be like this: The instability induces increased space-charge fields which produce radial fields which accelerate the particles radially and the magnetic field changes some of the radial velocity into angular velocity. These effects, however, are small in our experiments and the total axial kinetic energy remains virtually constant, while the angular and radial kinetic energies, although increasing substantially, remain much smaller than the axial kinetic energy. The transverse energies remain small because the diameters of the streams and the drift tube are smaller than any wavelength of interest so that no coherent oscillations are established in the transverse plane and the simple coupling mechanism described previously is not strong enough to increase the transverse kinetic energy.

V. SUMMARY

The results of the numerical experiments with a one-dimensional, disk model demonstrate that the saturation of growth of the convective two-stream instability is due to trapping and the development of a vortex structure in velocity space. Growth rates agree well with the predictions of the linear theory, but the essentially nonlinear phenomena of generation and amplification of harmonics are very strong. The streams exchange kinetic energy suddenly and become thoroughly mixed and thermalized, although the thermal velocities remain less than the velocity separation parameter. The results of numerical experiments with a two-dimensional ring model agree

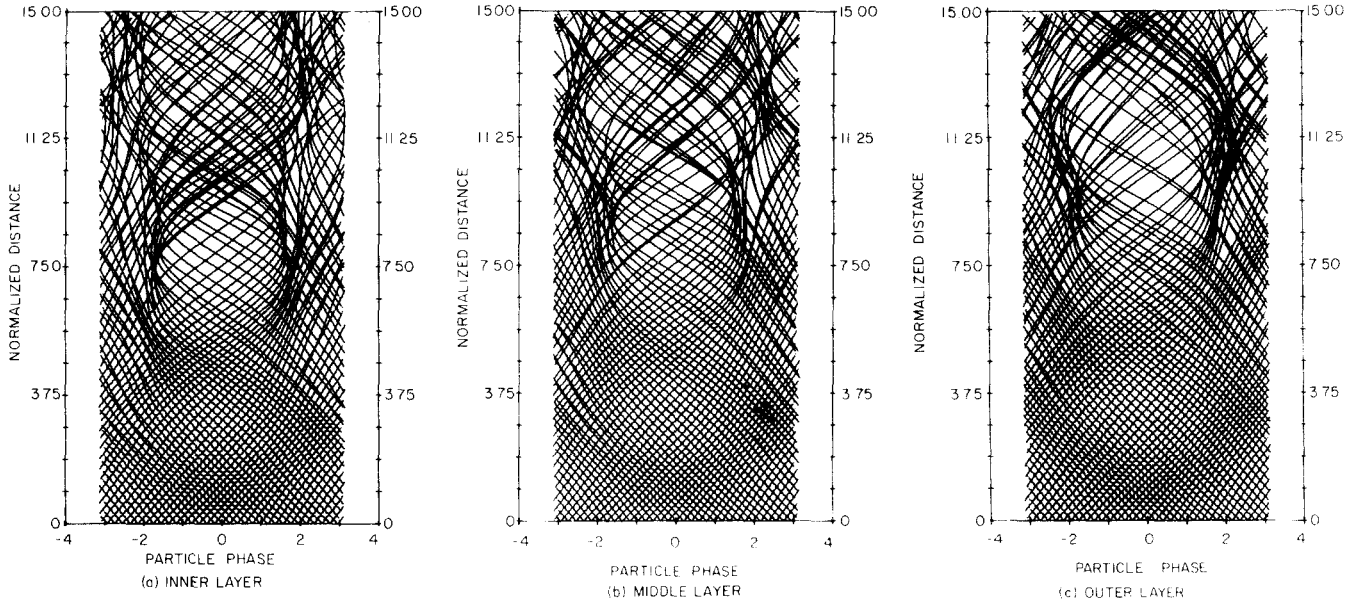

FIG. 9. Flight-line diagrams for particles at each layer of charge for experiment 4. ($M = 32, N = 3, N_x = 10$, $N_\Phi = 32$, $\omega_{p_1}/\omega = \omega_{p_2}/\omega = 0.1, \omega_c/\omega = 0.24$).

well with the comparable one-dimensional experiments, especially in terms of growth rates, harmonic generation and saturation. The axial electric field is practically independent of radius in the region occupied by the streams which justifies the use of one-dimensional models. The interaction is stronger for the rings closer to the axis and the inner particles exchange more kinetic energy and trapping occurs earlier inside the streams. The overall exchange of kinetic energy is reduced though and stream 1 remains the fast one and stream 2 the slow one. Only small gains in the transverse energy were observed, and it is believed that the complete exchange of kinetic energy seen in the one-dimensional experiments represents an artificial overshoot of the instability due to the one-dimensional formulation.[3] Due to the cost of the runs, the total number of particles had to be kept small and experiments were made with 192 and 320 particles. It is concluded that these numbers are sufficient to study

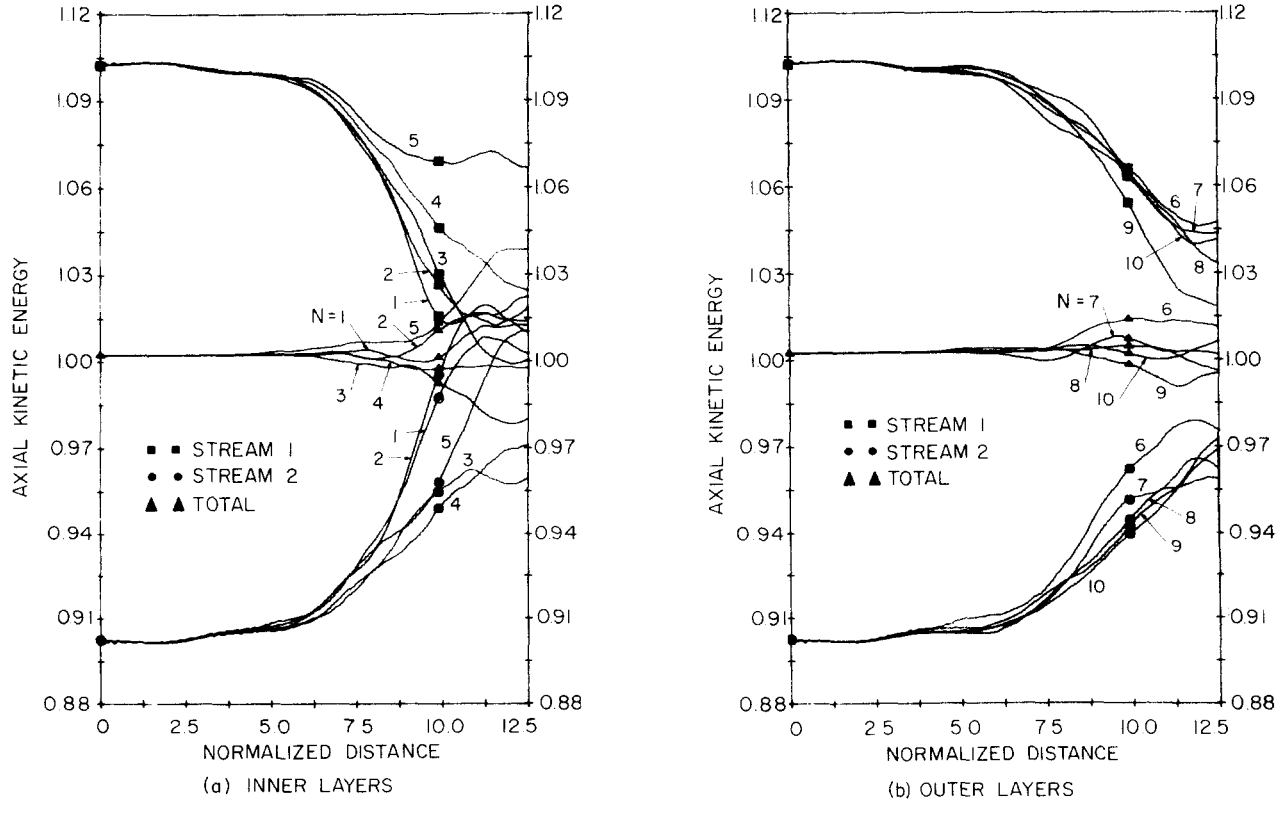

FIG. 10. Average axial kinetic energy of the particles in each of the layers of charge and for each stream in experiment 5. ($M = 16$, $N = 10$, $N_x = 20$, $N_\Phi = 16$, $\omega_{p_1}/\omega = \omega_{p_2}/\omega = 0.1$, $\omega_c/\omega = 0.24$).

phenomena occurring essentially in the axial direction. In order to simulate situations with radial velocity modulations or radial density variations it is suggested that at least 1000 particles ($2 \times 16 \times 32$) be used.

ACKNOWLEDGMENTS

The authors wish to thank Professor R. J. Lomax for valuable comments throughout the investigation.

This work was supported by the National Science Foundation under Grant No. GK-15689. One of the authors (J. B.-N.) was partially supported by the Michigan Memorial-Phoenix Project, Grant No. 354 and by CAPES—Coordenação do Aperfeiçoamento do Pessoal de Nivel Superior (Rio de Janeiro, Brazil).

APPENDIX

The axial and radial components of the normalized electric field used in this investigation are given by

$$E_y(y,x,\Phi) = -\frac{\eta}{2S^2 u_0 \omega} E_z(y,x,\Phi)$$

and

$$E_x(y,x,\Phi) = -\frac{\eta}{2S^2 u_0 \omega} E_r(y,x,\Phi),$$

where η is a positive number and E_z and E_r are obtained from the solution of Poisson's equation only. The Green's function technique is used, the fields for the delta-function ring are integrated over all particles and the integration is switched to the entrance plane to yield

$$E_z(y,x,\Phi) = -\frac{u_0}{\eta\omega}\frac{\omega_{p1}^2}{x_a^2}\int_0^{x_b} x'_{01}\,dx'_{01}\int_{-\pi}^{\pi}(1+b)(1+2Su'_{y10}) \times F_z(x,\Phi,x'_1,\Phi'_1)\,\mathrm{sgn}(\Phi-\Phi'_1)\,d\Phi'_{01} - \frac{u_0}{\eta\omega}\frac{\omega_{p2}^2}{x_a^2}\int_0^{x_b} x'_{02}\,dx'_{02} \times \int_{-\pi}^{\pi}(1-b)(1+2Su'_{y20})F_z(x,\Phi,x'_2,\Phi'_2)\,\mathrm{sgn}(\Phi-\Phi'_2)\,d\Phi'_{02}$$

and

$$E_r(y,x,\Phi) = -\frac{u_0}{\eta\omega}\frac{\omega_{p1}^2}{x_a^2}\int_0^{x_b} x'_{01}\,dx'_{01}\int_{-\pi}^{\pi}(1+b)(1+2Su'_{y10}) \times F_r(x,\Phi,x'_1,\Phi'_1)\,d\Phi'_{01} - \frac{u_0}{\eta\omega}\frac{\omega_{p2}^2}{x_a^2}\int_0^{x_b} x'_{02}\,dx'_{02} \times \int_{-\pi}^{\pi}(1-b)(1+2Su'_{y20})F_r(x,\Phi,x'_2,\Phi'_2)\,d\Phi'_{02},$$

where $x_a \Delta S\omega a/u_0$ and $x_b \Delta S\omega b/u_0$ are the normalized radii of the drift tube and of the streams. The subscripts indicate that the streams and $(1 + 2Su'_{y10})$ and $(1 + 2Su'_{y20})$ are the initial axial velocities. The primed variables indicate source points and the unprimed variables indicate field points. The function $\mathrm{sgn}(\Phi - \Phi')$ is defined as

$$\mathrm{sgn}(\Phi-\Phi') = \begin{cases} 1 & \text{if} \quad \Phi > \Phi' \\ 0 & \text{if} \quad \Phi = \Phi' \\ -1 & \text{if} \quad \Phi < \Phi' \end{cases}.$$

The functions F_z and F_r are the space-charge weighting functions and are defined as

$$F_z(x,\Phi,x',\Phi')\Delta \sum_{l=1}^{\infty} \frac{J_0[\mu_l(x/x_a)]J_0[\mu_l(x'/x_a)]}{[J_1(\mu_l)]^2} \times \exp\left(-\frac{\mu_l}{x_a}|y-y'|\right)$$

and

$$F_r(x,\Phi,x',\Phi')\Delta \sum_{l=1}^{\infty} \frac{J_1[\mu_l(x/x_a)]J_0[\mu_l(x'/x_a)]}{[J_1(\mu_l)]^2} \times \exp\left(-\frac{\mu_l}{x_a}|y-y'|\right),$$

where J_0 and J_1 are the cylindrical Bessel functions of order zero and one, and μ_l is given by the successive roots of $J_0(\mu_l) = 0$. The separation in distance $y - y'$ in the exponential is substituted by a separation in phase $\Phi - \Phi'$ by means of the first term of a Taylor series expansion.[6,9] The result is

$$|y-y'| \cong S(1 \pm b)[1 + 2Su_y(y,x'_0,\Phi'_0)]|\Phi-\Phi'|$$

and the upper sign applies when the source particle is in stream 1 and lower sign, when it is in stream 2. The phase differences used when computing the integrals for the fields are reduced to the interval $(-\pi,\pi)$ since periodicity in time is assumed. Also, the force between two particles decreases exponentially with distance and for phase separations larger than $\pm\pi$ they are neglected, thus justifying the integration from $-\pi$ to π over the source points.

The weighting functions are calculated beforehand for 60 equally spaced values of $|\Phi - \Phi'|$ in the interval $[0,\pi]$ and for all possible pairs (x,x') corresponding to the N_x points in which the radial direction is divided. The results are stored in the fast memory in table form. No interpolation is done and when calculating the contribution of a ring at (x',Φ') to the field at (x,Φ) the following steps are taken: The phase difference $|\Phi - \Phi'|$ is computed, the indices for N_x corresponding to x and x' are computed and the values of F_z and F_r corresponding to the triad $(x,x',|\Phi - \Phi'|)$ are retrieved from the tables. The series for the weighting functions are not uniformly convergent and their values for $\Phi - \Phi' = 0$ are obtained from physical considerations around the fact that the rings represent finite-sized lumps of charge that are tenuous and can pass through one another.[4] An immediate improvement would be to interpolate when referring to the tables (equivalent to the area-sharing procedure for the force of Refs. 3 and 4), but this was not attempted because of the increase in cost. However, interpolation was used when referring to the reduced table in the one-dimensional model.

To obtain the field for the one-dimensional case $E_z(y,x,\Phi)$ is integrated over the source points x_{01}' and x_{02}' since no radial variations now exist. The result still depends on x in the field point and to eliminate this dependence E_z is averaged over the area of the disk. As a result, the weighting function F_z depends only on $|y - y'|$ and this separation in distance is transformed into a separation in phase $|\Phi - \Phi'|$ in the same way as for the two-dimensional case.

[1] O. Buneman, Phys. Rev. **115**, 503 (1959).
[2] J. M. Dawson, Phys. Fluids **5**, 445 (1962); also, in *Methods in Computational Physics*, edited by B. Alder, S. Fernbach, and M. Rotenberg (Academic, New York, 1970), Vol. 9, p. 1.
[3] R. L. Morse and C. W. Nielson, Phys. Rev. Lett. **23**, 1087 (1969); **26**, 3 (1971).
[4] C. K Birdsall and D. Fuss, J. Comp. Phys. **3**, 494 (1969); A. B. Langdon, J. Comput. Phys. **6**, 247 (1970); C. K. Birdsall, A. B. Langdon, and H. Okuda in *Methods in Computational Physics*, edited by B. Alder, S. Fernbach, and R. Rotenberg (Academic, New York, 1970), Vol. 9, p. 241.
[5] A. T. Lin and J. E.Rowe, Phys. Fluids **15**, 166 (1972); **15**, 2034 (1972); J. A. Davis and A. Bers, in *Proceedings of the Symposium on Turbulence of Fluids and Plasmas* (Polytechnic Institute of Brooklyn Press and Interscience Publishers, New York, 1969), p. 87.
[6] A. T. Nordsieck, Proc. IRE **41**, 630 (1953); P. K. Tien, Bell Syst. Tech. J. **35**, 349 (1956); S. E. Webber, IRE Trans. Electron Devices **ED-5**, 306 (1958).
[7] R. W. Gould and M. A. Allen, in *Proceedings of the Fifth International Conference on Microwave Tubes* (Dunod, Paris, 1965); p. 445.
[8] G. T. Konrad and J. E. Rowe, in *Advances in Electronics and Electron Physics*, edited by L. Marton (Academic, New York, 1970), Vol. 29, p. 1.
[9] T. G. Mihran and S. P. Yu, J. Appl. Phys. **34**, 2976 (1963).
[10] T. G. Mihran, J. Appl. Phys. **37**, 624 (1966).
[11] J. E. Rowe, *Nonlinear Electron-Wave Interaction Phenomena* (Academic, New York, 1965), Chaps. 4 and 12.
[12] S. A. Self, J. Appl. Phys. **40**, 5217 (1969).
[13] R. J Briggs, *Electron-Stream Interaction with Plasma* (M.I.T. Press, Cambridge, 1969), p. 39.
[14] H. L. Berk and K. V. Roberts, Phys. Fluids **10**, 1595 (1967).